AD-A117 107 ARMY ELECTRONICS TECHNOLOGY AND DEVICES LAB FORT MON--ETC F/G 20/14
A NOVEL BEAM BUNCHING CONCEPT FOR MILLIMETER WAVE TUBES.(U)
JUN 82 P FISCHER, C BATES, J HARTLEY

UNCLASSIFIED NL

END
DATE FILMED
08-82
DTIC

Fischer, Bates, and Hartley

A NOVEL BEAM BUNCHING CONCEPT FOR MILLIMETER WAVE TUBES

*PAUL FISCHER, MR.
CALVIN BATES, MR.
JOSEPH HARTLEY, MR.
US ARMY ELECTRONICS TECHNOLOGY AND DEVICES LABORATORY
FORT MONMOUTH, N.J. 07703

INTRODUCTION

It can be demonstrated(1) that under suitable boundary conditions, a post-loaded reentrant RF cavity configuration such as that shown in Figure 1 can produce an oscillating electron sheet in its gap region when the cavity is excited by RF energy.

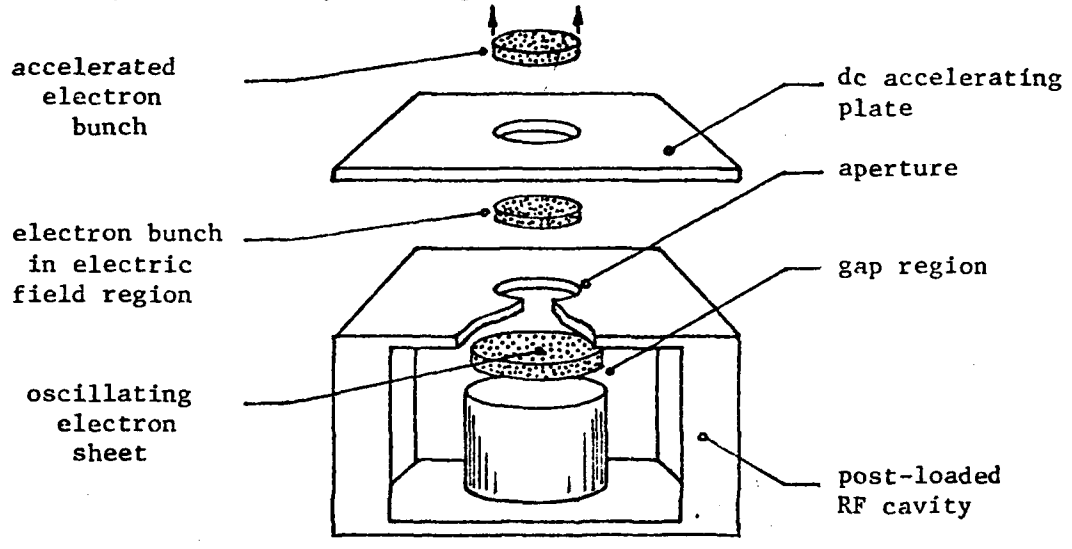

Figure 1. RF Electron Gun with dc Acceleration Region

The electron sheet is highly bunched and oscillates back and forth in the gap region at the fundamental frequency of the RF excitation. An aperture in the upper surface of the gap permits electron bunches from the oscillating sheet to escape from the cavity. One electron bunch is produced every RF cycle and each bunch (when viewed from the plane of the aperture) represents a pulse of unidirectional RF current. Thus, RF energy which excites the cavity is converted into electron beam energy and the cavity

configuration is, in effect, a non-thermionic source of pre-bunched electrons rich in RF harmonics. If the electron bunches emerging from the gap aperture are projected through a constant electric field region as shown in Figure 1, they will gain kinetic energy, which by virtue of the sharp, discrete, nature of the bunches can be converted into RF energy when the bunches are coupled to the fields of an RF output structure.

MATHEMATICAL MODEL AND ANALYSIS

The physical boundary conditions necessary to generate and control oscillating electron sheets in the cavity RF gap region can best be shown analytically with the aid of Figure 2 which is an idealized geometrical version of the RF gap and dc acceleration region of the gun.

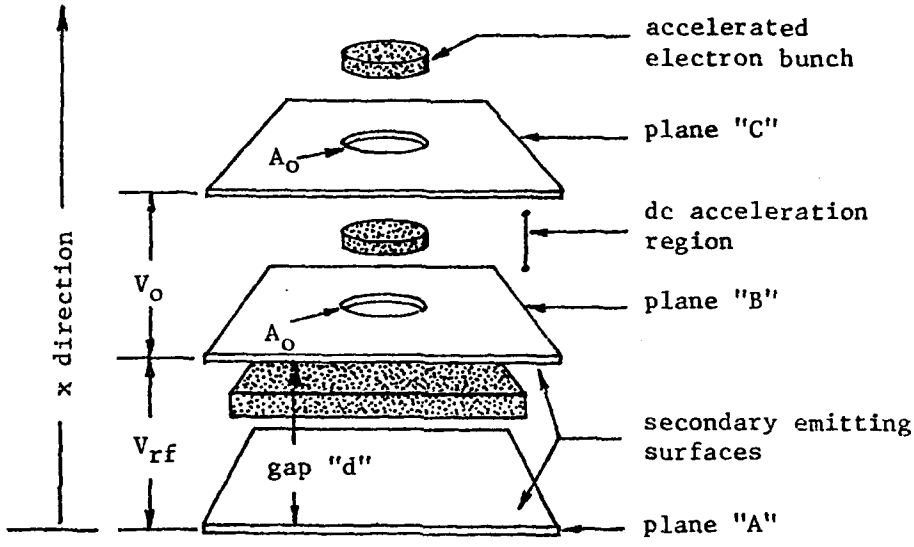

Figure 2. Analytical Model of RF Electron Gun

The RF gap region is modeled by two parallel planes, A, and B, with spacing, d, whose surfaces are capable of emitting secondary electrons when bombarded with primary electrons of sufficient energy. An RF voltage V_{rf}, is applied across planes A and B to generate and drive the electron sheet. The electron bunches are permitted to escape through an aperture of area, A_o, into a constant accelerating voltage region, V_o, bounded by planes B and C where the field imparts kinetic energy to the bunches. The accelerated electron bunches then pass through a second aperture of area, A_o, after which they can be utilized by an RF structure to convert their kinetic energy into RF output energy. An initial electron with velocity, v_o, starts out at plane A (x=0) and moves toward plane B whenever the RF field

is in the proper direction. The acceleration of the electron at any instant of time, t, is given (in M.K.S. Units) by,

$$\frac{d^2x}{dt^2} = \frac{e}{m} \frac{V_{rf}}{d} \sin(\omega t + \phi_0) \qquad \{1\}$$

where ϕ_o is the phase of the RF field when t = 0, x = 0; ω is the angular frequency of the RF field, and e/m is the charge-to-mass ratio of the electron. The velocity, v, of the electron at any position in the RF gap is obtained by integrating Equation {1} once with respect to time and is given by,

$$v = \frac{dx}{dt} = v_o + \frac{e}{m} \frac{V_{rf}}{d\omega} \{\cos \phi_0 - \cos(\omega t + \phi_0)\} \qquad \{2\}$$

Integrating once again with respect to time, one obtains the expression for the instantaneous electron position as follows,

$$x = \left(v_o + \frac{e}{m} \frac{V_{rf}}{d\omega} \cos \phi_0 \right) t + \frac{e}{m} \frac{V_{rf}}{d\omega^2} \{\sin \phi_0 - \sin(\omega t + \phi_0)\} \qquad \{3\}$$

Equations {1} to {3} contain implicit information needed to determine the conditions under which a planar RF gap region can generate and support an electron sheet which oscillates between the opposing faces of the gap at the frequency of the drive source as shown in Figures 1 and 2. In conjunction with the equations, one must use an empirically derived secondary emission curve (Figure 3) for the particular secondary emitters being employed on the gap surfaces. The figure illustrates a typical secondary emission curve in which primary electrons have sufficient energy to liberate secondaries whenever their impact energy in electron volts (ev) specified numerically by V_{imp}, is between V_I and V_{II}. V_I and V_{II} are the unity crossover points of the secondary emission ratio curve (ratio of secondary to normally incident primary electrons). In order for the sheet to exist, electrons within the sheet must traverse the gap distance d, (Figure 2) within, or very near one-half cycle of the drive oscillation frequency. When the sheet arrives at plane B, electrons within the sheet must have energies between V_I and V_{II} when they strike, so that they can produce secondary electrons to continue the process when the RF field reverses to draw the electrons back to plane A in the next half-cycle. Expressed mathematically, the transit time and impact boundary conditions are respectively,

$$t = \pi/\omega \qquad \{4\}$$

$$V_I < V_{imp} < V_{II} \quad \{5\}$$

for $x = d$ {6}

and $v_o = 0$ {7}

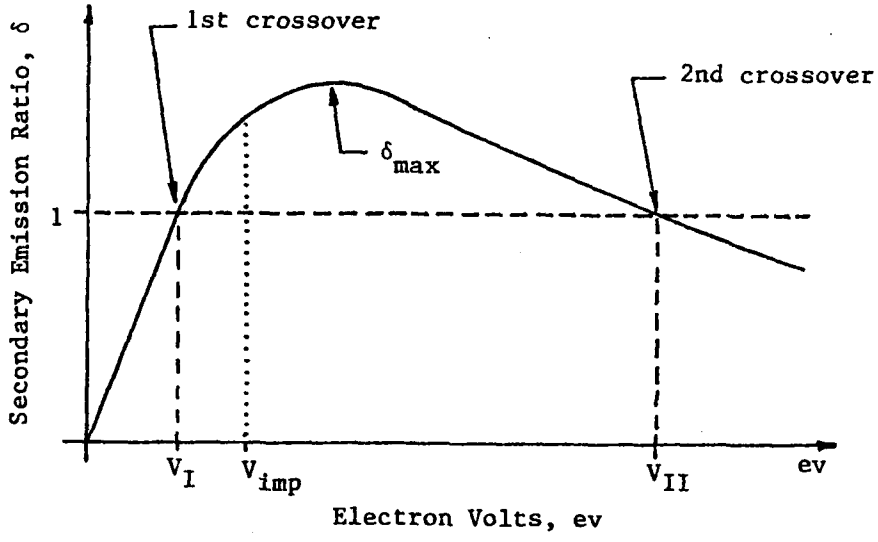

Figure 3. Generalized Secondary Emission Curve

Using Equation {4} through Equation {7} in conjunction with Equations {2} and {3} , yields, the gap dimension d, consistent with the required transit time condition shown in Equation {4}.

$$d = \sqrt{\frac{e}{m}\,\frac{V_{rf}}{\omega^2}\,\pi} \quad \{8\}$$

The impact voltage (V_{imp}) corresponding to that gap is given by,

$$V_{imp} = \frac{2}{\pi} V_{rf} \quad \{9\}$$

V_{imp} can be chosen independently from the experimental secondary emission curve (Figure 3); in practice it is preferable to pick V_{imp} at the peak, (δ_{max}), of the curve so that the maximum number of secondary electrons are obtained at impact each half-cycle. Once V_{imp} is specified, V_{rf} is determined by Equation {9}. The required V_{rf} is a function of the cavity (Figure 1) gap shunt impedance R_{sh}, and input drive power P_d, where,

$$P_d = \frac{V_{rf}^2}{R_{sh}} \qquad \{10\}$$

V_{rf}, therefore, can be obtained by suitable cavity design for R_{sh} or adjustment of the drive power, P_d or both. Since the shunt impedance and drive power can be chosen independently of frequency (2), V_{rf} is independent of frequency. Furthermore, the physical phenomenon of electron bunching is not dependent on frequency, but is determined by the phase of the electron leaving one surface, and the phase and energy with which it strikes the opposite surface. The electron bunching process occurs as a result of the phase and energy selection of electrons existing in the gap region. Thus, a scaled experimental model (for example 5 Gigahertz (GHz)) can be designed and built to verify the foregoing analysis for millimeter wave lengths. Once the shunt impedance and drive power are specified to produce the required RF voltage (V_{rf}), the gap spacing (d) is determined by Equation {8} for any desired drive frequency, ω.

The cyclic electron build-up and bunching process described in the foregoing analysis is a special case of the secondary electron resonance phenomenon (also called multipactor) extensively described in the scientific literature (see, for example, Reference 3). Equations {8} and {9} which specify the gap dimension and the corresponding electron impact energy (V_{imp}) were derived for an initial electron velocity and departure time of zero. In actuality, electrons are emitted over a range of departure times (departure angle) and arrive at the opposite gap face over a range of arrival times (conduction angle). The departure and arrival times are normally clustered about $t = 0$ and $t = \pi/\omega$, respectively, for practical cases. In addition, the emitted electrons have initial velocities corresponding to energies of 0 to 30 ev (4) with the maximum number of electrons emitted at approximately 2-5 ev. Iterative calculations using Newton's method (5), for Equations {2} and {3}, show that electrons having initial energies of up to 5 ev, will have departure and arrival times which cluster about $t = 0$ and $t = \pi/\omega$ respectively. The increased initial velocities will cause corresponding increases in departure and conduction angles. Experimental devices to be discussed in this report employ a gap spacing of 0.020 inches (0.508mm), with surfaces of either silver or copper (see Reference 4 for experimental secondary emission curves). For this gap, calculations yield values of approximately 30 degrees for the departure and conduction angles.

For a gap which can support secondary electron resonance, the electron sheet builds up rapidly once RF power is applied (normally in less than 10 cycles) until the space charge in the sheet becomes bounded by the perveance of the gap (6). Perveance in this case defines the maximum peak RF current I_p (in amperes) obtainable through the aperture at plane B (Figure 2). The peak RF current is represented by rectangular pulses (solid lines) as shown in Figure 4.

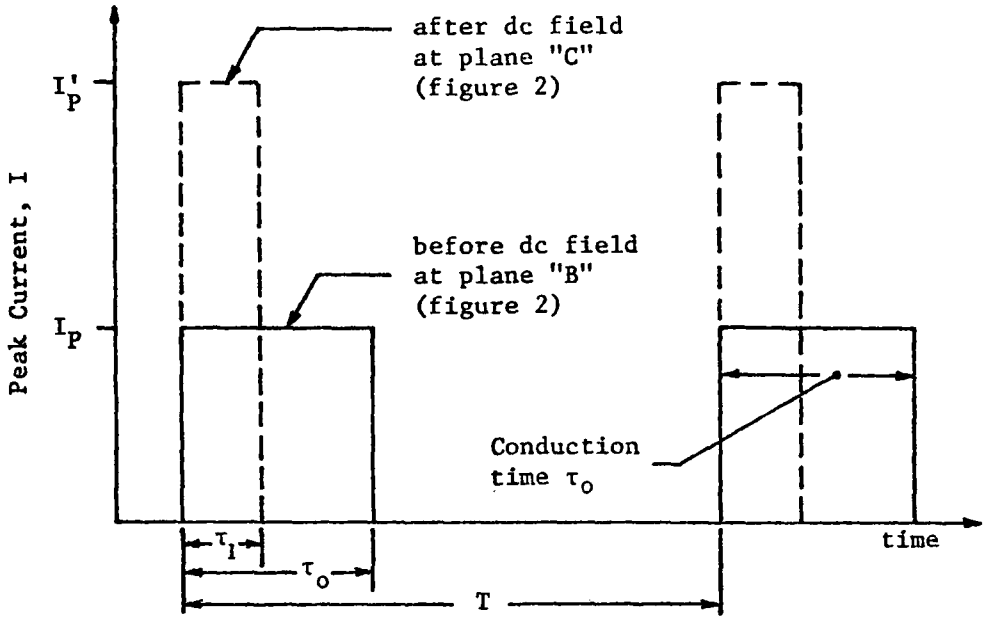

Figure 4. Peak Currents Before and After Acceleration of Electron Bunches

It should be noted here that the peak RF currents and powers represented in Figures 4 and 5 occur at each RF cycle, and should not be confused with the conventional terminology which defines peak current and peak power produced by power bursts (pulses) containing many RF cycles. The peak RF current is given by,

$$I_p = 2.334(10^{-6}) \frac{A_o}{d^2} V_{rf}^{3/2} \qquad \{11\}$$

The peak instantaneous power in the bunch can also be represented by a

rectangular pulse as shown in Figure 5 (solid line), with the peak power P_B in the bunch at plane B being given by,

$$P_B = (V_{imp})(I_P) \qquad \{12\}$$

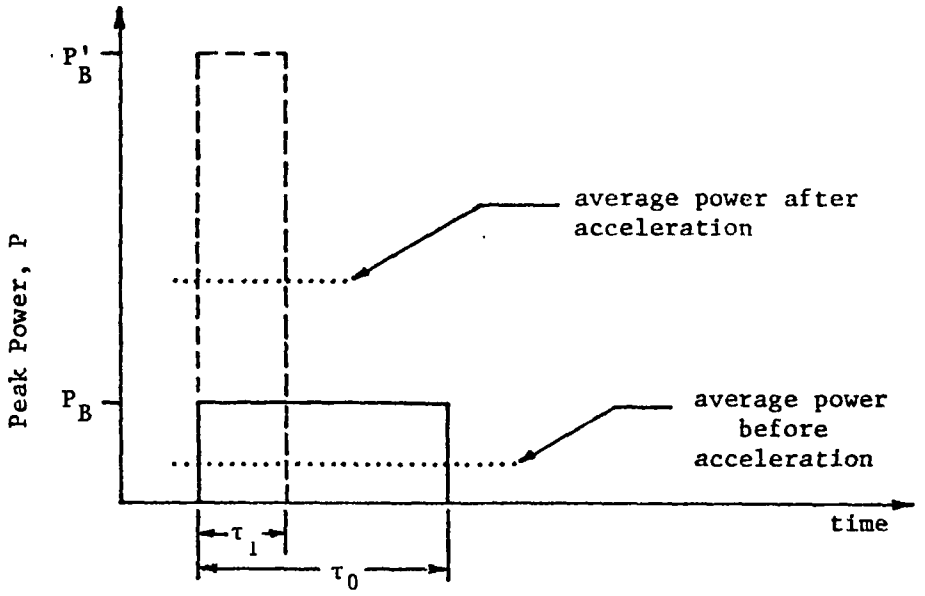

Figure 5. Peak Powers Before and After Acceleration of Electron Bunches

After the bunch is accelerated through the dc acceleration region to gain energy, its peak power, P_B', (dashed line) is given at plane C by,

$$P_B' = (G_P)(P_B) \qquad \{13\}$$

where G_P is the peak power gain given by,

$$G_P = 1 + \frac{V_o}{V_{imp}}\left(1 + \sqrt{\frac{V_o}{V_{imp}}}\right) \qquad \{14\}$$

and the corresponding peak current gain G_I, is,

$$G_I = 1 + \sqrt{\frac{V_o}{V_{imp}}} \qquad \{15\}$$

The increased peak current, I_p', and peak power, P_B', at plane C are shown with dashed lines in Figures 4 and 5 respectively. For the experimental tube prototype to be discussed, $G_I = 3.2$ and $G_p = 12.2$ for $V_o = 1500$ volts and

V_{imp} = 300 volts (for copper). Thus, a substantial increase in the kinetic energy of the bunches can be obtained with a moderate accelerating dc voltage. The average power gain Gavp produced by the dc fields is,

$$G_{avp} = \frac{V_o}{V_{imp}} + \frac{1}{1 + \sqrt{\frac{V_o}{V_{imp}}}} \qquad \{16\}$$

and for the prototype tube Gavp = 5.3. Figure 5 also indicates that the average power is increased after acceleration (dotted lines).

The peak currents shown in Figure 4 can be represented by a Fourier series (7). For the purposes of this paper, we are interested only in the fundamental component of the RF current at plane C and its amplitude I_1, is given by,

$$I_1 = \frac{2}{\pi} I_p G_I \sin(\pi \frac{\tau_1}{T}) \qquad \{17\}$$

where τ_1, is the pulse width of the current at plane C, and T is the period of the fundamental RF drive. The ratio of the pulse width τ_1 at plane C, to the pulse width, τ_o, at plane B is,

$$\frac{\tau_1}{\tau_0} = \frac{1}{1 + \sqrt{\frac{V_o}{V_{imp}}}} \qquad \{18\}$$

and shows the effect of the dc accelerating field (V_o) on the pulse widths of instantaneous current and power. Neglecting RF circuit losses, one can show that the maximum RF power gain G_{rf} (with respect to the fundamental component) achieveable with the electron bunches is,

$$G_{rf} = 1 + \frac{V_o}{V_{imp}} \qquad \{19\}$$

and the maximum efficiency, η, is,

$$\eta = \frac{1}{1 + 2\frac{V_{imp}}{V_o}} \qquad \{20\}$$

Thus, the maximum limitations of RF power gain and efficiency (neglecting the RF losses in the RF input and output structures) with the gun/bunching configuration as shown in Figures 1 and 2, are functions of the impact voltage (V_{imp}) and the dc accelerating voltage (V_o). From Equations {19} and {20}, it follows that in order to optimize gain and efficiency, one must minimize V_{imp} and maximize V_o. V_{imp} in practice for presently useable secondary emitting materials (copper, silver, gold, platimum, magnesia-gold-cermets, etc.) is between 35 and 1000 ev. Power-supply/modulator, voltage breakdown, and electron de-bunching considerations affect the

choice of V_o. In practice voltages as high as 25 kilovolts (kV) can be easily utilized to achieve very high gain and efficiency. However it can be shown that even voltages of approximately 5 kV will produce devices having useable gain and efficiency. For example, for copper, the peak δ in Figure 3 is approximately 1.25 at V_{imp} = 500 V. If one chooses V_o = 5,000 V, the maximum achievable power gain and efficiency are 10.4 dB and 83 percent respectively. Note that both maximum gain and efficiency are independent of frequency and improve with the dc accelerating voltage. In an actual device the power gain and efficiency are reduced somewhat by the RF losses in the input cavity and the RF output structure.

PRELIMINARY EXPERIMENTAL MODEL AND RESULTS

An experimental multipactor collector model shown in Figure 6 was designed and constructed at 5 GHz to demonstrate the RF to dc conversion features of the theoretical concept. Initial evaluations using a continuous wave (CW) input power level of 400 milliwatts (mW) produced current at the accelerator/collector electrode, and verified the 400 mW turn-on design value. The gap in this model was 0.020 inches (0.508 mm), and the secondary emitting surfaces were silver. The input power was increased to 1.5 watts to obtain sufficient RF drive to perform current collection experiments under stable conditions. The calculated current level for this design was approximately 8.5 mA for a 1.5 watt input, and the experimental value obtained was approximately 1 mA dc with a collector voltage of 100 V dc. The lower current obtained was most likely due to the RF

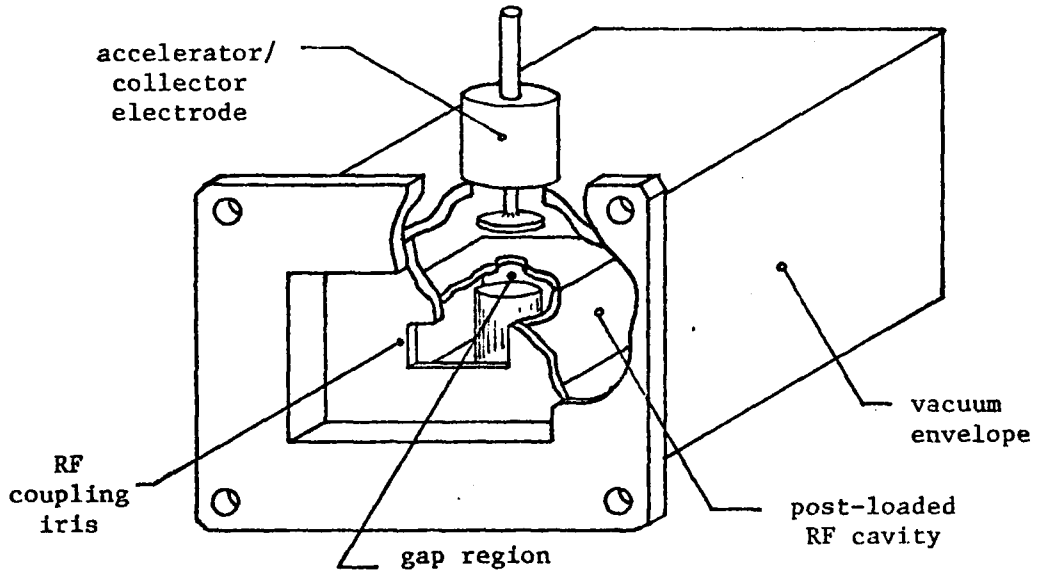

Figure 6. Experimental Multipactor Collector Model

losses in the cavity, and the large amount of outgassing noticed during operation which may have contaminated the secondary emitting surfaces. Pulsed drive tests were also performed, and Figure 7 shows the detected current pulse and detected RF input pulse. The duty was maintained at low level (<0.01) to minimize outgassing effects.

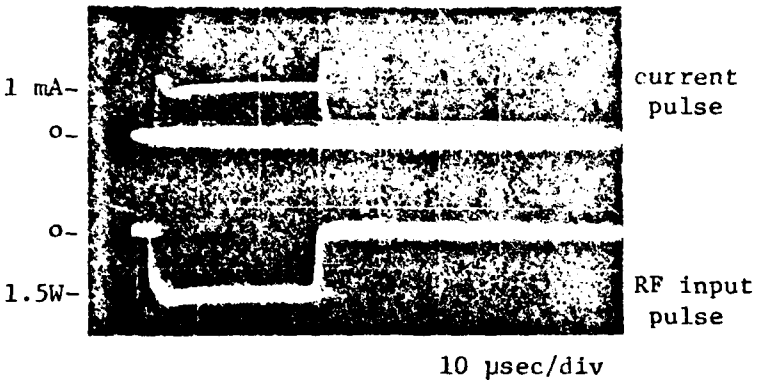

Figure 7. Detected Current Pulse and RF Input Pulse of Multipactor Collector Model

Again a peak current of approximately 1 mA was achieved with a peak power input of 1.5 watts. Note that the two pulses occur simultaneously showing that the turn-on and turn-off of the output current is controlled by the RF input pulse.

For further confirmation of the theory, the impact voltage (V_{imp}) of the electron bunches was measured by biasing the collector negative with respect to the aperture plane until current was cut-off. The cut-off occurred at approximately 300 volts which agrees within 10 percent of the calculated value of 289 volts.

RF PROTOTYPE DESIGN

A new tube prototype (8) was designed, based on the encouraging results obtained with the preliminary gun model. The new 5 GHz prototype is shown schematically in Figure 8. The tube consists of an RF input cavity which generates the electron sheet. An electron beam sieve, through which the electron bunches are driven, separates the input and output cavities. The RF output cavity ingeniously combines both the RF output interaction and the dc acceleration regions by virtue of an isolated accelerator electrode which is inserted into the hollow post of the output cavity. The input and output cavities are electrically discharged machined (EDM'ed) copper blocks as shown in Figure 9. Also shown are the accelerator electrode and the beam sieve plate.

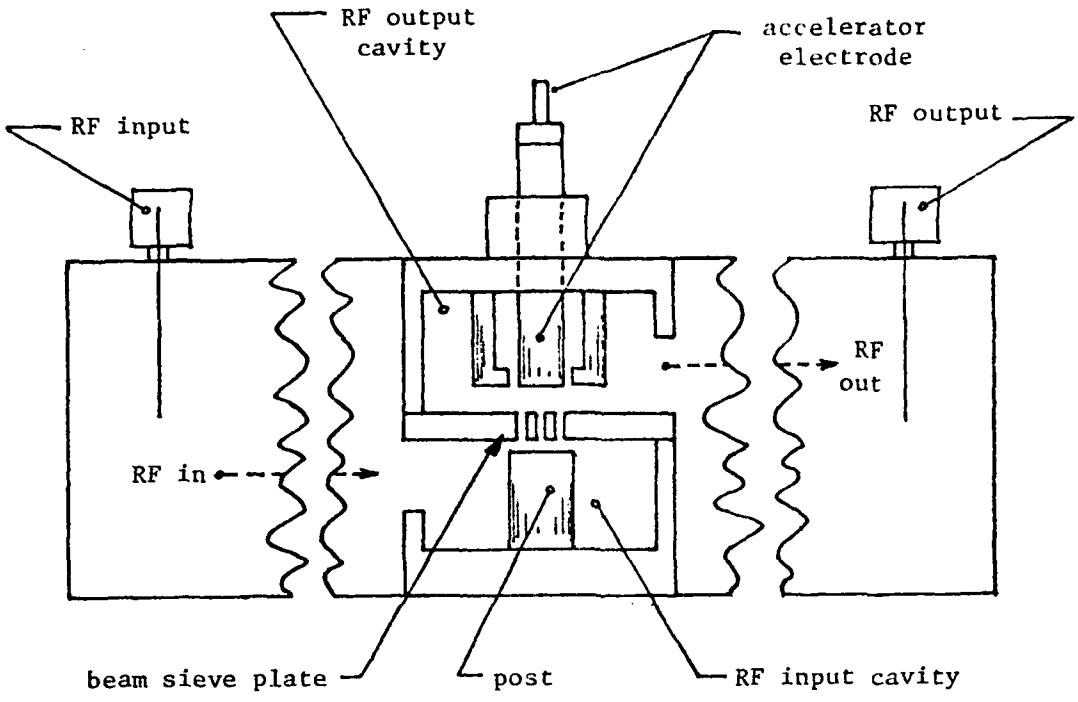

Figure 8. Internal Configuration of 5 GHz Prototype Tube

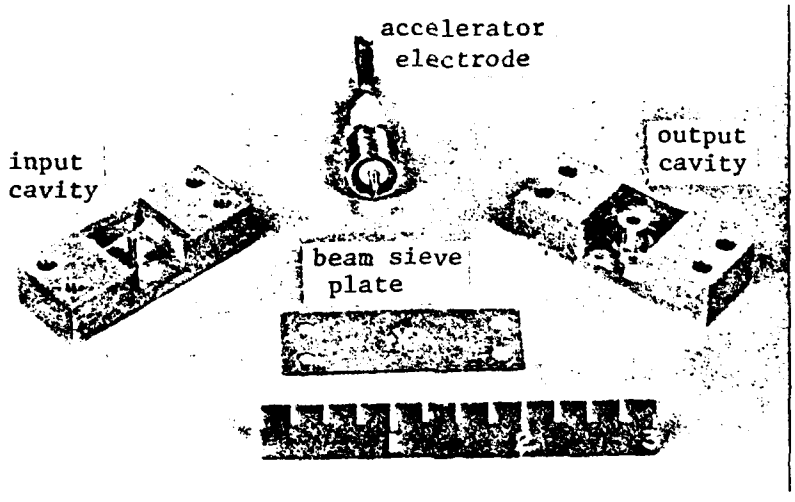

Figure 9. View of Internal Components of 5 GHz Prototype Tube

Figure 10 shows the input (lower), and output (upper) cavities stacked together with the accelerator electrode inserted in the output cavity. The RF input coupling iris and the post of the input cavity are visible. Cold tests of the RF subassembly were performed using standard network analyzer techniques to assure frequency coincidence of the input and output cavities with the beam-sieve plate and accelerator electrode in place. A single-hole beam-sieve plate which was described in the theory, provides the proper aperture for the electron bunches, however, the cold tests showed that the RF isolation between cavities was only 10 dB. In order to improve the RF isolation a multiple-aperture beam-sieve plate, using seven smaller holes, was fabricated and cold tests showed an improvement to 25 dB RF isolation. An RF isolation of at least 20 dB was considered important to separate the effects of the cavities during future hot tests, and to assure that the output power to be observed would be a function of the RF gain mechanism, and not a function of RF leakage between the cavities. Moreover, the multiple-aperture beam-sieve will be more effective than the single-aperture sieve in coupling the RF fields in the output cavity to the electron beam, since the RF fields generated between the post and metallic surfaces of the sieve will be in very close proximity to the electron beam. The multiple-aperture beam-sieve will also enhance the operation of the input cavity, by providing a more uniform RF field distribution in the gap region, than that attainable using a larger single-aperture sieve.

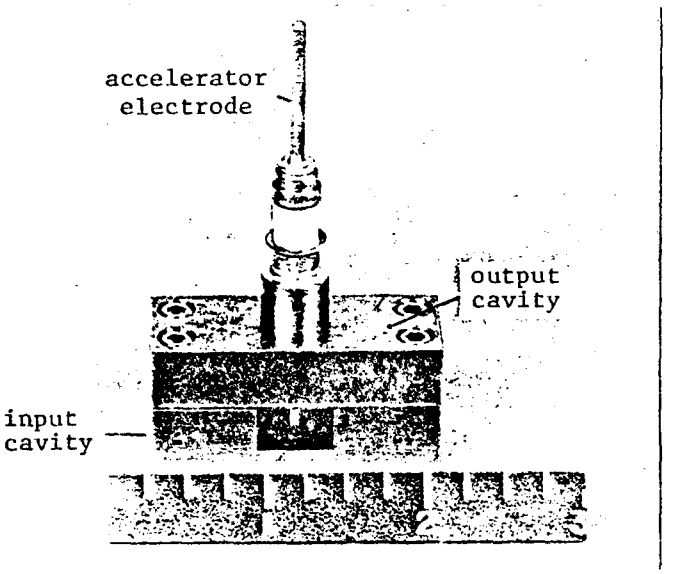

Figure 10. RF Subassembly for 5 GHz Prototype Tube

The RF subassembly is inserted into the center of the waveguide body, where it is held in place by the accelerator electrode. The complete prototype tube (Figure 11) uses standard RF vacuum connectors which are brazed to the waveguide body at the same time the accelerator electrode, vacuum fittings, and end plates are brazed. The tube will be capable of a bakeout temperature of 500°C.

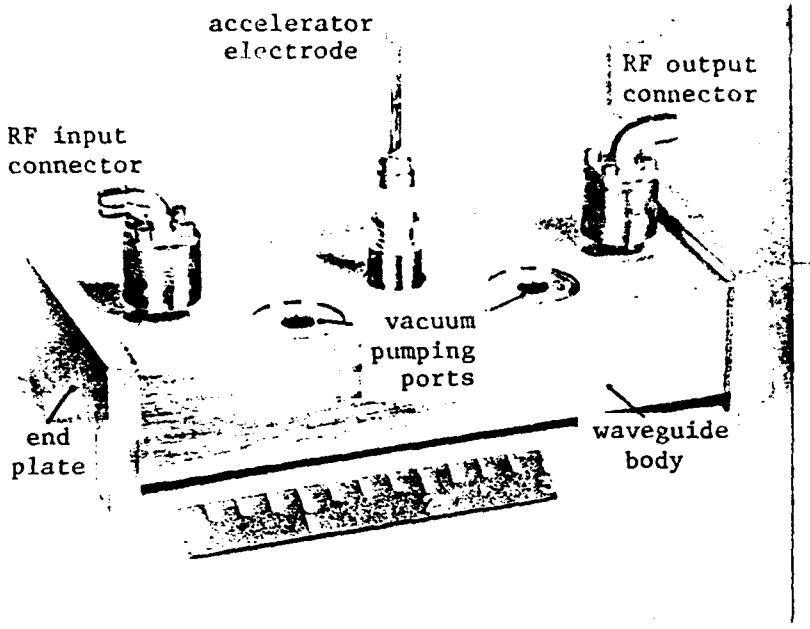

Figure 11. Complete Assembly of 5 GHz Prototype Tube

The design parameters for this tube which utilizes copper gap surfaces are listed below.

Frequency	5 GHz
Multipactor gap, (d)	0.020" (0.5mm)
Electron impact, voltage (V_{imp})	300 volts
Gap RF voltage	471 volts
Accelerator voltage (V_o)	1.5 kV
RF gain	8.2 dB
Efficiency	70%
Input power	1.5 watts
Output power	10 watts
Volume	15 cubic inches (250 cc)
Weight	1.5 pounds (0.7 kg)

This feasibility prototype has been designed and fabricated to demonstrate the formation of the electron bunches, and the gain mechanism generated by interaction with the RF fields. Future multi-stage models designed around the concept will demonstrate enhanced capabilities for specific Army system application.

CONCLUSIONS

A unique electron beam bunching concept has been presented, analyzed, and applied to the development of a novel tube approach. The analysis provides a design base for a new class of millimeter wave tubes. These tubes will be compact, lightweight, reliable, and low cost due to the simplicity of design and construction in comparison to conventional thermionic tubes with magnets. Furthermore, the analysis shows that useful RF gain and efficiency can be achieved at moderate accelerator voltages, which makes possible the use of simplified, low cost, lightweight, power supplies and modulators.

Theoretical considerations have been confirmed by evaluation of an experimental multipactor collector model. Furthermore, the results have demonstrated that the electron bunching can be generated and controlled by low RF drive (less than 1 watt), and that the currents generated are useful for new tube approaches. Although experiments were conducted at 5 GHz, the results are applicable for devices operating at millimeter wave frequencies.

A 5 GHz prototype tube design has been formulated, and component parts for the tube have been machined and cold-tested. The tube is presently being assembled for subsequent processing and evaluation. It is expected that this simplified, two-cavity design will demonstrate useful gain and efficiency, and provide the technology base for developing new tube prototypes for Army millimeter wave system applications.

REFERENCES

(1) C. Bates et. al., "Multipactor Electron Gun for Millimeter Wave Tubes," IEDM Technical Digest, pp 339-343, Dec 1981

(2) T. Moreno, Microwave Transmission Design Data, McGraw-Hill Book Co., Inc., First Edition, pp 228-230, 1948

(3) A. J. Hatch, "Electron Bunching in the Multipacting Mechanism of High-Frequency Discharge," Journal of Applied Physics, Vol. 32, No. 6, pp 1086-1092, June 1961

(4) H. Bruining, Physics and Applications of Secondary Electron Emission, Pergamon Press, Ltd., First Edition, pp 27-31, 104-107, 1954

(5) D. McCracken, FORTRAN With Engineering Applications, John Wiley & Sons, Inc., pp 44-52, 1967

(6) W. J. Gallagher, "The Multipactor Effect," IEEE Transactions on Nuclear Science, Vol. NS-26, No. 3, pp 4280-4282, June 1979

(7) S. Goldman, Frequency Analysis Modulation and Noise, McGraw-Hill, pp 25-27, 1948

(8) C. Bates, "Multipactor Beam Amplifier," Invention Disclosure, Docket No. 2447, filed May 1981


TE
MED
8